JOURNAL OF MATERIALS SCIENCE **38** (2003) 1679–1687

Microstructural evaluation and phase transformation of recast layers in electrical discharge machined dual phase Fe-Mn-Al alloy

JYH-WEI LEE
Department of Mechanical Engineering, Tung Nan Institute of Technology, Shen-Ken, Taipei, 222, Taiwan
E-mail: jefflee@mail.me.tnit.edu.tw

The electrical discharge machining process is an effective way to machine hard alloys. A homogenized dual phase Fe-24.0%Mn-8.3%Al-5.0%Cr-0.38%Si-0.34%Mo-0.45%C (wt%) alloy casting piece was employed to study the phase transformation and microstructure phenomena of recast layers by means of electrical discharge machining. The wave-like recast layers appear with micro cracks. The thickness of the recast layer increases with pulse duration. When the pulse duration ranges from 200 to 300 μs, the discharge current has no influence on the thickness of the recast layer. The copper concentration is high in the recast layer caused by the melting of the copper electrode. The copper contents of the recast layer increase with the pulse duration and the discharge current.

The novel solidification microstructures of the recast layer can be classified as (1) a dense and fine dendritic outermost sublayer, (2) a coarse dendritic intermediate sublayer and (3) an innermost γ recast zone. The average chemical composition of the recast sublayers is Fe-19.007%Mn-8.377%Al-2.981%C-4.505%Cr-0.627%Cu-0.377%Mo-0.376%Si (wt%). The novel structure of the recast sublayer is identified as $(Fe,Mn)_3AlC_x$, which was formed due to the re-melting of the matrix and the carburization of the cracked dielectric fluid. The precise lattice parameter, a_o, of the $(Fe,Mn)_3AlC_x$ phase measured by extrapolation against $\cos^2\theta/\sin\theta$ is 0.3801 nm. The microhardness of the recast layers is as high as Hmv574 due to the existence of $(Fe,Mn)_3AlC_x$ carbide. © *2003 Kluwer Academic Publishers*

1. Introduction

Electrical discharge machining (EDM) is a nontraditional manufacturing process, using the energy of electric discharges to melt and to remove the surfaces from work pieces. During the EDM process, there is no contact between the electrode and the work piece, which implies no cutting force produced on the work piece. The EDM process is also not restricted by the hardness, strength or toughness of work pieces. This makes it most suitable for high hardness, high toughness materials that are hard to machine by traditional manufacturing processes.

The surface of electrical discharge machined material is formed by accumulations from discharge cycles and is full of craters, chimneys, droplets and microcracks. Although local surface material is melted or even vaporized and removed by the pressure of dielectric fluid vapor during EDM, about 85% of the melted material may resolidify rapidly on the surface of the work piece. The accumulated new structure on the surface is called the "recast layer" or the "white layer" due to its non-revelation by etching [1, 2]. The recast layer is full of craters and microcracks that make for poor surface precision and shortness of service life.

Fe-Mn-Al alloy steel was invented more than one hundred years by Hadfield [3]. In this alloy system, manganese substitutes for nickel, and chromium is replaced by aluminum to achieve properties comparable to traditional SUS 304 stainless steel [4]. The surface chromization characteristics [5], oxidation performance and oxidation induced phase transformation phenomena of Fe-Mn-Al alloy steels were studied by Duh *et al.* [6, 7]. According to Zuidema's work [8], the high work-hardening rate of austenitic Fe-Mn-Al alloy steel was caused by high contents of manganese, aluminum and carbon comparable to that of SUS 301 and 201 stainless steels [9]. Due to the toughness and hardness, machining of this alloy by traditional manufacturing processes is a tough and tedious job. The attrition among cutting tools is also expensive. Consequently, electrical discharge machining has become an alternative choice to machine such hard alloys. However, the electrical discharge machining process on Fe-Mn-Al alloy has never been studied in the literature. Nor has any suitable electrical discharge machining parameter for Fe-Mn-Al alloy been investigated. The surface microstructures of the Fe-Mn-Al alloy after EDM have never been revealed. The objective of this study was to determine the electrical discharge machining

0022–2461

parameters for Fe-Mn-Al alloy steel. The dependence of morphology, microhardness, chemical composition and phase transformation phenomena of the recast layer with respect to pulse duration and discharge current were also studied.

2. Experimental procedure

The Fe-Mn-Al alloy was melted, in a 100-kilogram induction furnace, in air. 1008 low carbon steel, pure manganese, ferromanganese, pure aluminum, ferrochromium and ferromolybdenum were used as raw materials. The liquid steel was then poured into ceramic shell molds. The 75 mm long, 15 mm diameter casting rods were homogenized at 1100°C for 5 hours. 10 mm thick discs were cut from the homogenized casting rods. The chemical composition of Fe-Mn-Al alloy was analyzed as Fe-24.0%Mn-8.3%Al-5.0%Cr-0.38%Si-0.34%Mo-0.45%C (in wt%) by the wet chemical method. The structure of this alloy was further identified by use of an X-ray diffractometer (Rigaku, Model DMAX-B) equipped with Cu target and graphite single crystal monochrometer. The working conditions were 40 KV and 100 mA.

The EDM experiment was conducted after the disc surface was ground with #1200 SiC abrasive papers. The electrode used in EDM was copper with 99.9% purity. The dimensions of the electrode were 8 mm diameter, 50 mm long. The electrical discharge fluid was kerosene. The generator used was kept in an iso-frequent mode. The pulse-on voltage and the total EDM time were 35 volts and 15 minutes, respectively. Variations of pulse current (I_e) and pulse duration (t_e) are indicated in Table I.

The electrical discharge machined Fe-Mn-Al alloy discs were ultrasonically cleaned in acetone for 10 minutes to remove contaminants. The surface morphologies of specimens were further observed by means of Scanning Electron Microscopy (SEM). The surface structures were identified with an X-ray diffractometer again. Each disc was cut vertically, using a water-cooled precision cutting machine to reveal the cross section of its EDMed surface. The specimen was then hot mounted, ground and up to 0.3 μm polished away by alumina powder. An ultrasonic cleaner was used to remove the residual alumina powder. Each specimen was etched in 5% Nital solution (5% HNO_3, 95% Alcohol). The thickness of the recast layer was observed with an optical microscope and measured at 50 μm intervals. The microhardness of the recast layers, the matrix adjacent to the recast layer and the matrix several hundred micrometers away from the surface in specimens B and J were measured with a Vickers microhardness tester (Matsuzawa, DMH-1) under 1 N load.

TABLE I EDM parameters[a] and average thickness of recast layers of Fe-Mn-Al alloy cast piece

Specimen designation	Discharge current, I_e (A)	Pulse duration, t_e (μs)	Average thickness of recast layer (μm)	Standard deviation (μm)
A	5	50	18.53	5.86
B	5	80	21.89	7.63
C	8	150	27.33	9.73
D	8	200	28.27	10.61
E	10	200	28.56	9.55
F	10	300	32.09	10.69
G	12	200	28.72	13.51
H	12	300	31.66	10.55
I	15	200	32.26	7.88
J	15	300	33.46	16.7

[a] The pulse-on voltage 35 V, total EDM time 15 min.

The morphology of the recast layer was further examined with an SEM. The elemental redistribution of recast layers was detected with an Electron Probe Microanalyzer (EPMA, JEOL JXA-8800M) by quantitative analysis of concentration for Fe, Mn, Al, C, Mo, Si, Cr and Cu with the aid of a ZAF-corrected program.

3. Results and discussions

3.1. Microstructural morphologies of electrical discharge machined specimens

The homogenized Fe-Mn-Al alloy cast piece was identified as having ferritic and austenitic dual phases structure by X-ray diffractometry. The typical secondary electron images (SEI) of surface morphologies after electrical discharge machining of specimens B ($I_e = 5$A, $t_e = 80$ μs) and J ($I_e = 15$A, $t_e = 300$ μs) are shown in Fig. 1a and b. It's obvious that the craters on

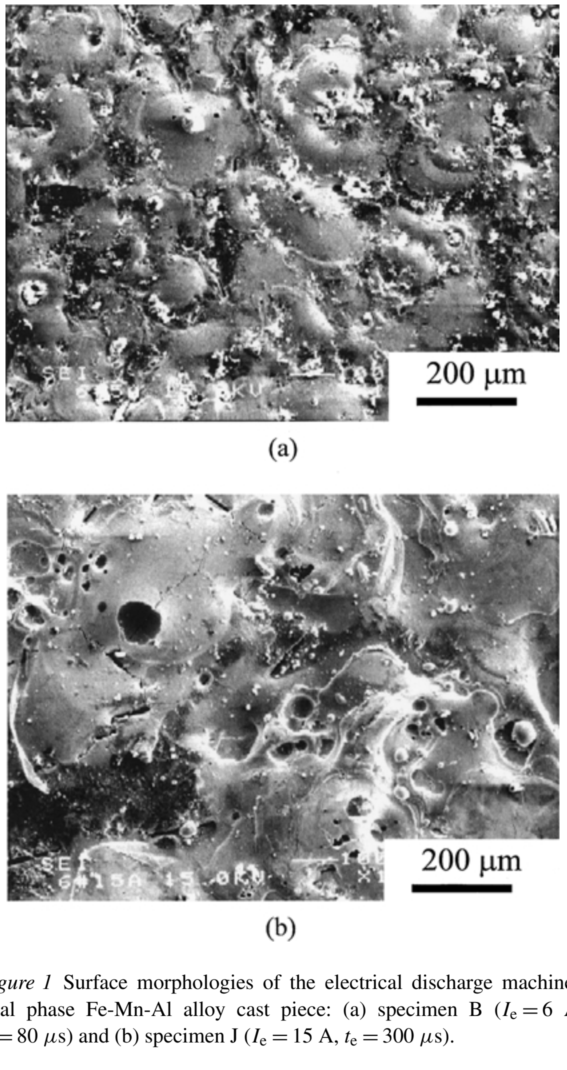

(a)

(b)

Figure 1 Surface morphologies of the electrical discharge machined dual phase Fe-Mn-Al alloy cast piece: (a) specimen B ($I_e = 6$ A, $t_e = 80$ μs) and (b) specimen J ($I_e = 15$ A, $t_e = 300$ μs).

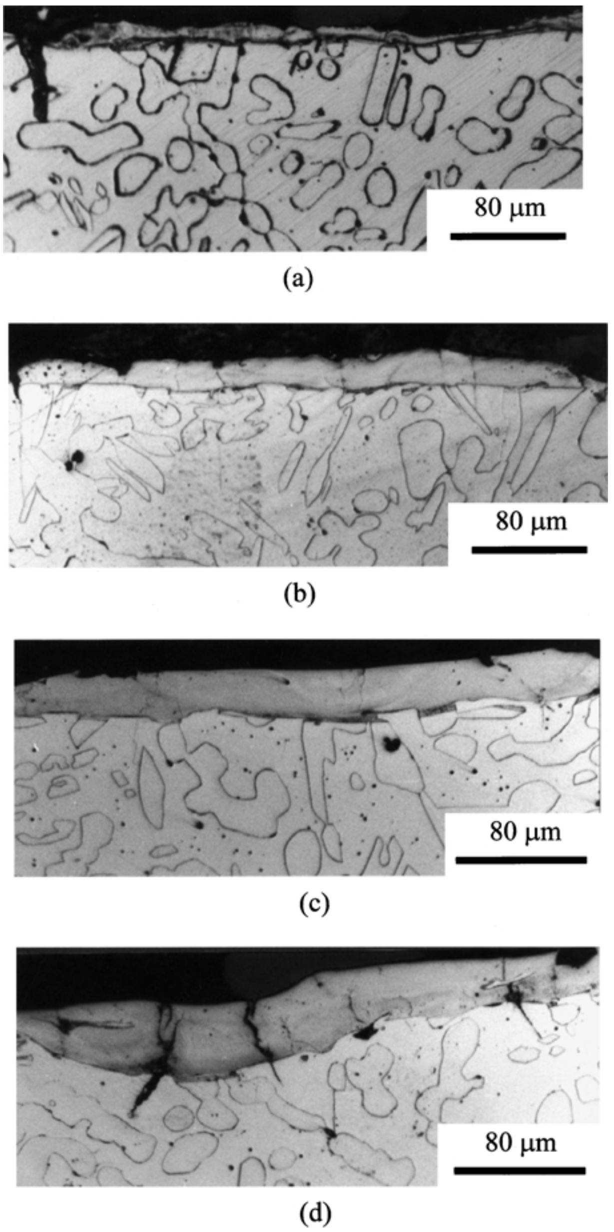

Figure 2 Optical micrographs of recast layers in electrical discharge machined dual phase Fe-Mn-Al alloy cast piece: (a) specimen B ($I_e = 6$ A, $t_e = 80$ μs), (b) specimen E ($I_e = 10$ A, $t_e = 200$ μs), (c) specimen H ($I_e = 12$ A, $t_e = 300$ μs), and (d) specimen J ($I_e = 15$ A, $t_e = 300$ μs).

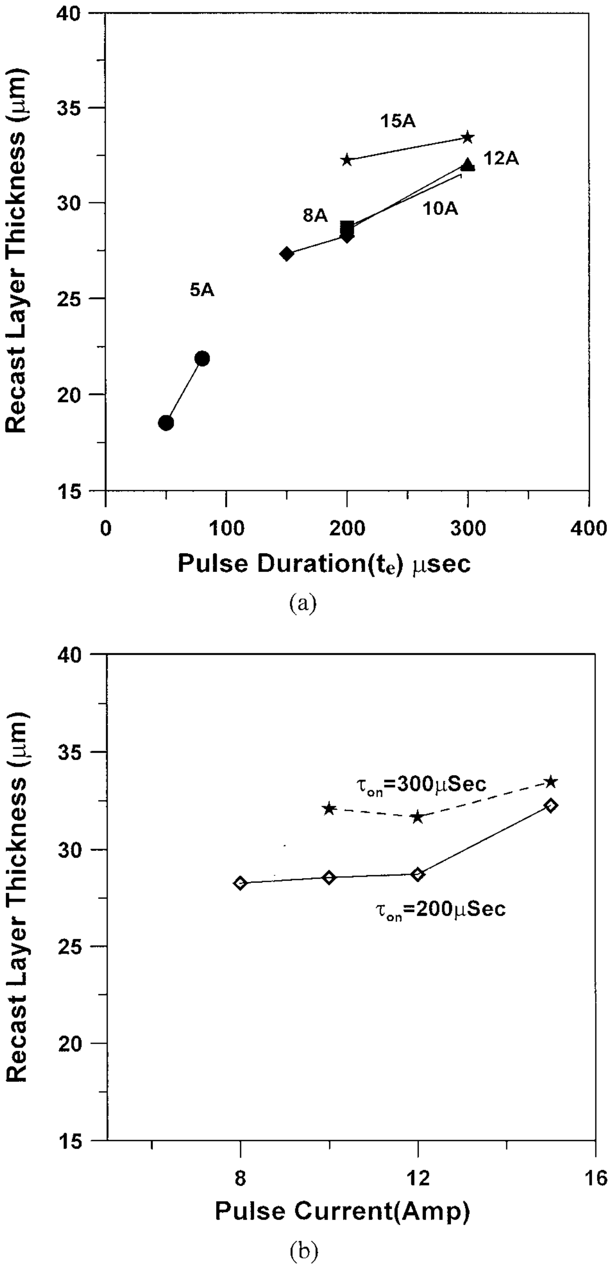

Figure 3 Dependence of recast layers thickness on (a) pulse duration and (b) pulse current.

the surfaces become greater and deeper as the t_e and I_e increase. The surface defects such as pockmarks, chimneys, global debris and microcracks become worse as t_e and I_e increase.

Fig. 2a, b, c and d represent typical optical micrographs of the recast layers of specimens B, E, H and J, respectively. It is evident that the recast layers appear as nonuniform and wave-like morphologies. There are many microcracks penetrating the recast layer which even cleave into the adjacent matrix phase. The average thicknesses and standard deviations of recast layers are also listed in Table I. The standard deviations of recast layers are almost one-third of the average thickness, indicating wave-like morphologies. In general, the thickness of the recast layers increases with increasing pulse duration and current.

The relation of recast layers' thickness versus pulse duration and pulse current are plotted in Fig. 3a and b. With pulse currents ranging from 8 to 12 A., the thickness of the recast layer (T) versus the pulse duration (t_e) obeys an exponential relationship evaluated by the regression method.

$$T(\mu\text{m}) = 8.1922 \times t_e^{0.2372} \tag{1}$$

As the pulse duration is maintained for 200 μs, the thickness of the recast layer (T) versus pulse current (I_e) exhibits another exponential relationship.

$$T(\mu\text{m}) = 26.069 \times I_e^{0.0392} \tag{2}$$

The fact that the thickness of the recast layer increases with increasing discharge energy has been described in the literature [1, 2, 10, 11]. From the above equations, the t_e term has greater influence than the I_e term on the value of recast layer thickness (T). When the pulse current is kept constant, the average thickness of the recast layer increases with the pulse duration. However, the thickness of the recast layer remains almost constant as the pluse currents increase from 8 to 12 A. According to Mamlis' study [11], pulse duration is the major influence factor on the thickness of the recast layer, while the pulse current plays a minor role. Based on the results from Table I and Fig. 7, the pulse duration is also a more pronounced factor on the recast layer thickness in the EDM process of dual phase Fe-Mn-Al alloy casting in this study.

The microcracks formed on the specimen surface were caused by thermal and transformational stress generated in the material during EDM processing [1, 12]. The depth of surface damage increases with increasing discharge energy [1, 2, 10, 11]. The microcracks cleaving into the matrix have detrimental effects on the mechanical properties. The service life of materials with microcracks will be reduced tremendously, especially in fatigue and corrosion environments. Detailed observation of the morphologies of the recast layers in Fig. 2a and d shows that microcracks penetrate the recast layers and cleave deep into the matrix. However, microcracks of specimens E and H (i.e., $I_e = 10$–12 A, $t_e = 200$–$300\ \mu$s) in Fig. 2b and c are found to hardly penetrate into the matrix. It is believed that the discharge energy produced under subsequent EDM parameters, $I_e = 10$–12 A and $t_e = 200$–$300\ \mu$s, is intermediate and under acceptable conditions removes the surface materials, while not generating excess damage to the matrix. With such working parameters, the thickness of recast layers remains almost constant and microcracks produced are restricted to the recast layers. Therefore, the electrical discharge machining parameters, $I_e = 10$–12 A and $t_e = 200$–$300\ \mu$s are suitable for the processing of the dual phase Fe-Mn-Al alloy steel cast in this study.

3.2. Cross sectional morphological characteristics and microhardness of recast layers

The cross sectional morphologies of the recast layer of specimen H ($I_e = 12$ A, $t_e = 300\ \mu$s) are shown in Fig. 4a, b, c and d. Two kind of sublayers are observed in the right portion of Fig. 4a (a) which can be divided into a dense and fine dendritic sublayer in the outermost region and a coarse dendritic sublayer inside. A definite planar internal growth front exists between these two sublayers. In fact, two equal thickness sublayers are found in Fig. 4b. Columnar dendrites with different orientations are observed in both sublayers. A distinct microstructure region with small nuclei of dendrites and fine, parallel dendrite arms is clearly visible beneath the two sublayers and on the top of an austenitic phase. This region exhibits a melted-in γ recast zone feature in Fig. 4b. The melted-in γ recast zone also exhibits a planar interface apparance. An obvious porosity in the interface of the recast sublayer and the matrix is shown in Fig. 4c. Two sublayers are deposited on the matrix surface. The fine and coarse columnar dendrites are visible in these sublayers. A long strip of matrix material is trapped in the coarse columnar dendritic intermediate sublayer in Fig. 4c. A fine dendritic outermost sublayer, coarse columnar dendritic underlying sublayer and melted-in γ recast zone are also observed in Fig. 4d,

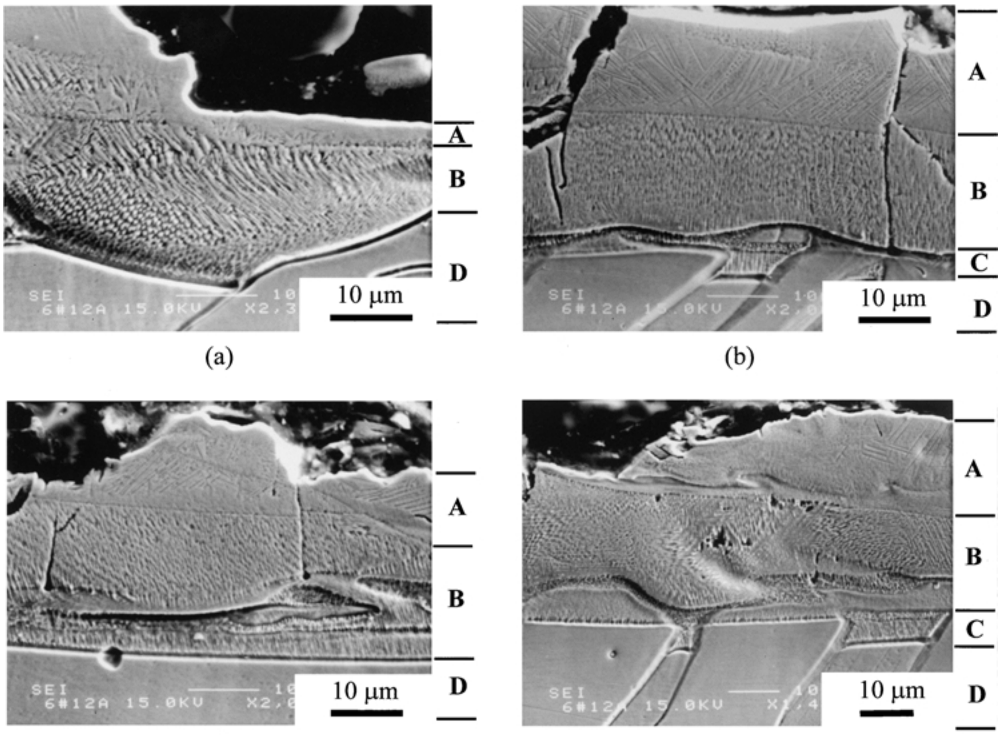

(a) (b)

(c) (d)

Figure 4 Solidification microstructures of recast layer of specimen H: (a) two sublayers (one thin, one thick), (b) two sublayers with identical thickness, (c) a porosity in the interface between intermediate sublayer and matrix, and (d) several pores in intermediate sublayer. (Marker A: outmost sublayer, B: intermediate sublayer, C: innermost γ recast zone, D: matrix.)

which shows severe porosities. It is obvious that the melted-in γ recast zones are only found to stretch into the austenitic phase adjacent to the recast layer.

Lim *et al.* [1] found recast layers on tool steel in three different types: thick multilayer, intermediate single layer, and thin featureless. They defined three discernible topmost, intermediate and innermost sublayers in the intermediate single layer. In this study, similar solidification microstructures of the recast layer in Fe-Mn-Al alloy can also be classified as (1) a dense and fine dendritic outermost sublayer, (2) a coarse dendritic intermediate sublayer and (3) an innermost γ recast zone. Dendritic microstructures with different orientations are observed in these two sublayers and the γ recast zone. The interface between the intermediate sublayer and the matrix is almost planar. The innermost "melted-in" γ recast zones only stretch into the austenite phase and show different morphologies than the other sublayers and matrices. This specific morphology of the innermost recast zone has never before been reported in the literature. The formation mechanism of the γ recast zone is still not clear. However, the phenomenon of a "melted-in" phase of the innermost γ recast zone is possibly attributed to the higher thermal conductivity of the γ phase.

More detailed solidification microstructures of recast layers of specimen H are shown in Fig. 5. The planar internal growth interface of the thin outermost sublayer and the columnar coarse dendritic intermediate sublayer is observed in Fig. 5a. The planar internal growth front of two columnar dendritic sublayers in different orientations is also found in Fig. 5b. Interfaces among the columnar dendritic intermediate sublayer, the innermost γ recast zone and the adjacent matrix are clearly visible in Fig. 5c. The γ recast zone stretches several micrometers into the austenite phase. Two particles with matrix microstructure are observed between the columnar dendritic intermediate sublayer and innermost γ recast zone. A straw matting structure that is the characteristic structure of $(\mathrm{Fe,Mn})_3\mathrm{AlC}_x$ carbides in coarse dendritic intermediate sublayer is present in Fig. 5d.

The metallurgy of EDM surfaces has been studied by many researchers [1, 13–16]. Many distinguishable surface layers have been reported. A poorly defined boundary of the heat-affected zone was also found between the recast layer and the matrix in high chromium white iron by Tabrett [16]. However, the matrix adjacent to the recast layer, or the so-called heat-affected zone is not found even by chemical etching in the EDMed Fe-Mn-Al alloy in the present work.

The microhardness of recast layers tested on the cross-sectional specimens B and J are H_{mv} 574 and 548, respectively. The microhardness of ferrite and austenite phases in the matrix are H_{mv} 318 and 344, individually. It's apparent that the recast layer is 1.6 times harder than the matrix. The reasons for the hardening of the recast layer will be discussed later. The microstructure and micro hardness of the matrix adjacent to the recast layer shows no difference as compared with the matrix a hundred micrometers away from the EDBed surface. No phase changes, metallographic difference or micro hardness variation in the matrix adjacent to the recast layer are revealed.

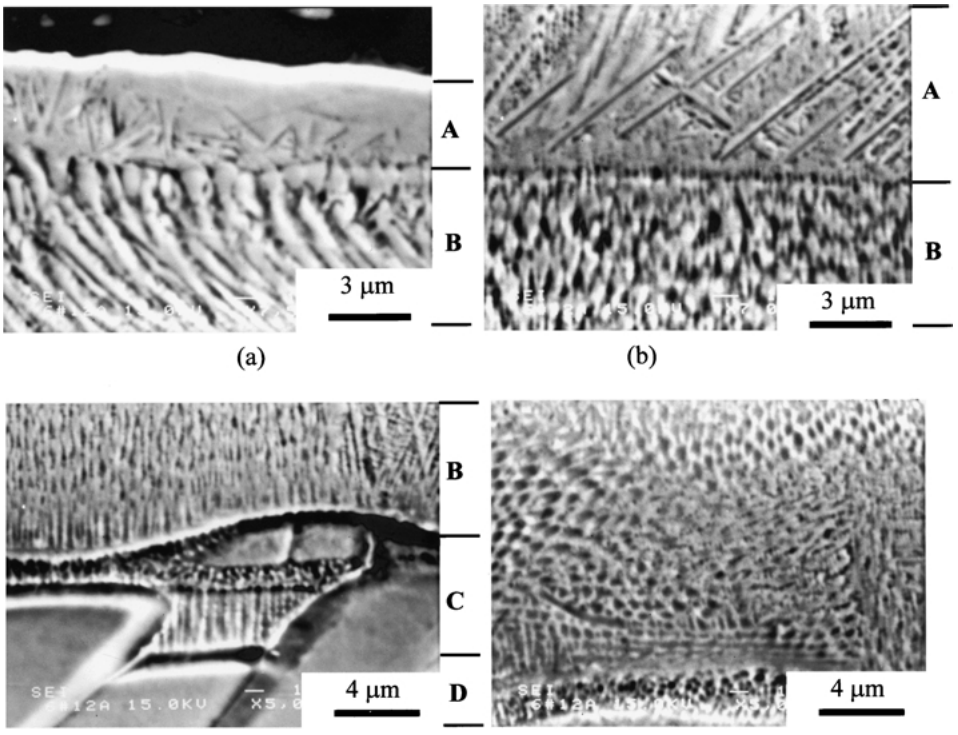

(a) (b)

(c) (d)

Figure 5 Solidification microstructures of recast layer of specimen H: (a) interface of a thin outmost and a thick intermediate columnar dendritic sublayers, (b) interface of outmost and intermediate dendritic sublayers, (c) interfaces among intermediate columnar dendritic sublayer, innermost γ recast zone and adjacent matrix, and (d) straw matting structure in coarse dendritic intermediate sublayer. (Marker A: outmost sublayer, B: intermediate sublayer, C: innermost γ recast zone, D: matrix.)

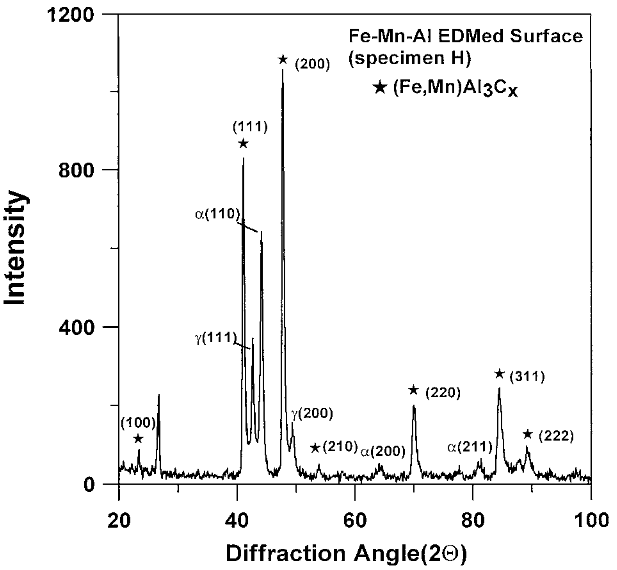

Figure 6 The X-ray diffraction pattern of electrical discharge machined surface of specimen H.

3.3. Phase identification and chemical composition analysis of recast layer

The X-ray diffraction patterns of the electrical discharge machined surface of specimen H are plotted in Fig. 6. The major diffraction peaks of the EDMed surface are identified as the κ carbide of (Fe,Mn)$_3$AlC$_x$. The austenite and ferrite phases of the matrix are also revealed. The X-ray diffraction patterns of the recast layers of different EDM condition specimens exhibit the same results.

The secondary electron images and concentration profiles of the recast layer and the adjacent matrix of two different regions, denoted as region I and II in the specimen H, are shown in Figs 7 and 8, respectively. Almost no chemical composition differences between outermost and intermediate sublayers are found. The average chemical compositions of recast sublayers, γ recast zones, ferrite and austenite in the matrix, for regions I and II of specimen H are listed in Table II. The average chemical composition differences between the recast sublayers and the γ recast zone are only in manganese, carbon and copper. 4.28 wt% higher in manganese and 0.873 wt% lower in carbon are observed in the γ recast zone. The average concentration of copper in the recast sublayers of region II is about 0.628 wt% and drops to 0.091 wt% in the γ recast zone and then decreases to 0.024 wt% in the ferrite matrix. In region II, the average concentration of carbon in the recast sublayers is as high as 2.694 wt%, which is identified as the (Fe,Mn)$_3$AlC$_x$ carbide phase. The concentration of carbon gradually decreases to 1.874 wt% in the γ recast zone and then decreases to 1.508 wt% and 0.717 wt%, respectively, in the austenite and ferrite phases adjacent to the recast layer. The concentration profile of manganese shows inverse variation when compared to that of carbon. In region II, the average concentrations of aluminum in the (Fe,Mn)$_3$AlC$_x$ carbide phase recast sublayers and the γ recast zone reach 8.35 wt% and then change to 7.395 wt% and 9.227 wt% in the austenite and ferrite phases adjacent to the recast layer.

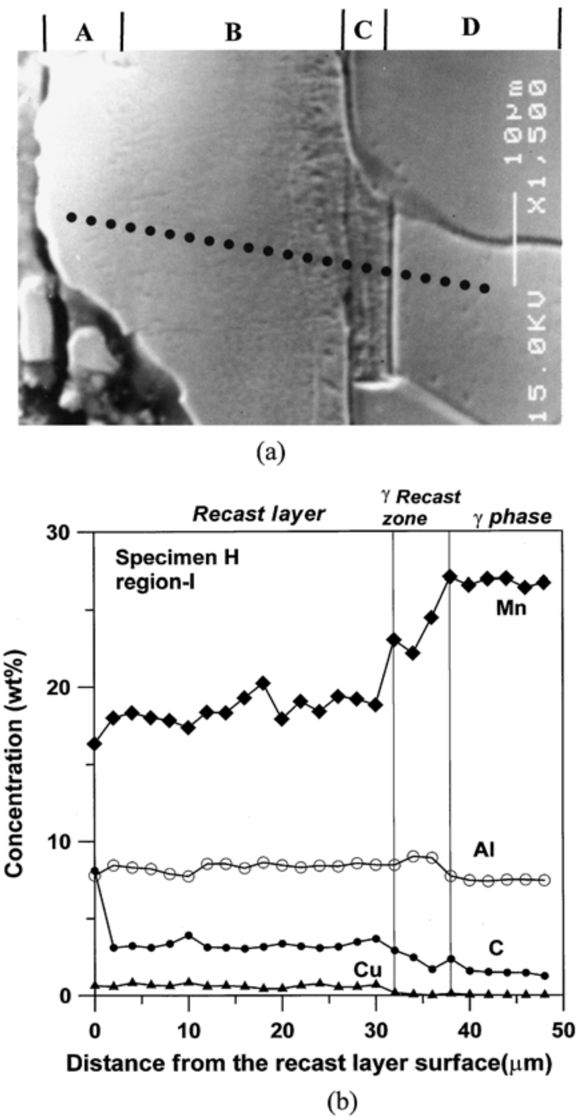

(a)

(b)

Figure 7 Morphology and concentration profile for specimen H: (a) SEI image of quantitative analysis region I and (b) concentration profiles of recast layer region I. (Marker A: outmost sublayer, B: intermediate sublayer, C: innermost γ recast zone, D: matrix).

The concentration profiles of chromium, silicon and molybdenum show little variation in the recast sublayers, γ recast zone and adjacent ferrite and austenite phases.

The elements' migration from electrode material to work piece in the EDM process has been studied [14, 17–19]. A cupronickel surface was formed on the high nickel alloys in the EDM process with a copper electrode [17]. The EDMed stainless steel surface was turned to a coated surface with an electrode component [19]. In this study, it is found that an appreciable amount of elemental copper, about 0.628 wt% at maximum, has migrated from the tool electrode to the recast layer of specimen H. However, the average copper concentration in the recast layer is only 0.08 wt% for specimen B. It is argued that the higher discharge energy generated in specimen H melted or evaporated more electrode material than was the case for specimen B. Some of the melted or evaporated copper was carried away by dielectric fluid; the remainder resolidified with the workpiece material to form the recast layer.

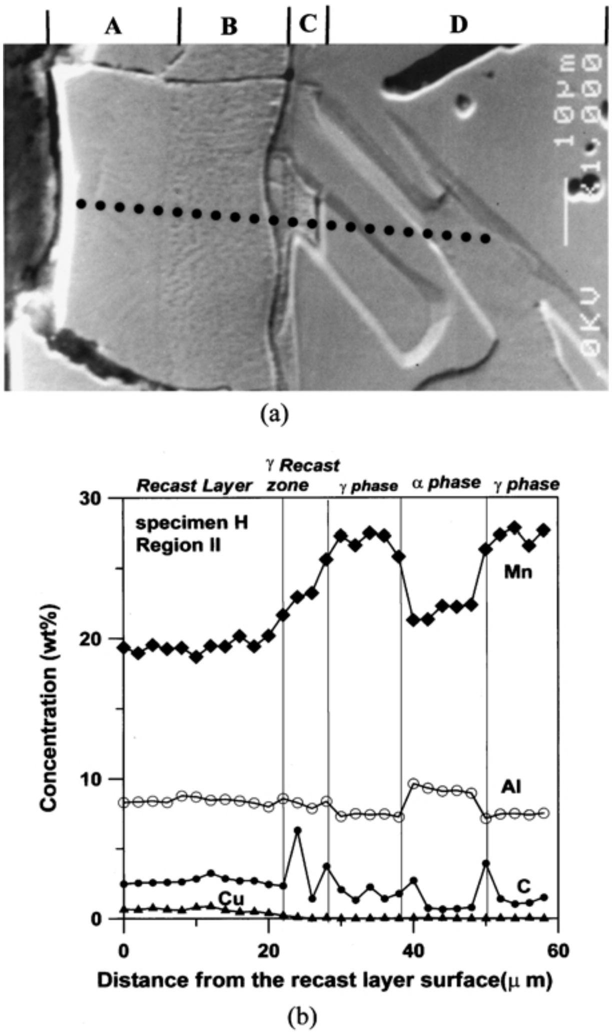

(a)

(b)

Figure 8 Morphology and concentration profile for specimen H: (a) SEI image of quantitative analysis region II and (b) concentration profiles of recast layer region II. (Marker A: outmost sublayer, B: intermediate sublayer, C: innermost γ recast zone, D: matrix.)

Although copper contents are high in the recast layer (0.627 wt%) and the γ recast zone (0.081 wt%) in specimen H, no copper related new phase is found from the X-ray data in Fig. 6.

The average chemical composition of the recast sublayers of specimen H is Fe-19.007%Mn-8.377%Al-2.981%C-4.505%Cr-0.627%Cu-0.377%Mo-0.376%Si (in wt%) measured by EPMA. It is concluded that the high carbon content of the recast layer was from the cracking of kerosene. The carburization effect even makes the carbon concentration of adjacent austenite and ferrite phases up to 1.508 wt% and 0.717 wt%, respectively in region II. To compare the carburization effect, the carbon contents of austenite and ferrite phases in the matrix several hundred μm away from the surface were measured as 0.750 wt% and 0.318 wt%, respectively. A similar phenomenon was observed by Kruth *et al.* [15] in the EDM processing of steel, in which Fe_3C carbides in columnar, dendritic structures were found in the recast white layer machined in an oil dielectric. Carbide formation was also noted on the surfaces of pure titanium [17], uranium [20] and zirconium [21] as a result of EDM in hydrocarbon dielectrics. The high hardness values of the recast layers were also reported by other researchers [16–18, 22]. In the present study, the higher microhardness of recast layers of specimen B and H are also evidence for the existence of an $(Fe,Mn)_3AlC_x$ carbide phase in recast sublayers. The hardness of the $(Fe,Mn)_3AlC_x$ phase was measured by Hale [23] and Sato [24]. In their studies, the $(Fe,Mn)_3AlC_x$ phase was formed by aging treatment at 550°C for long time. However, the hardness of the $(Fe,Mn)_3AlC_x$ phase aged for 10000 minutes only reaches to about Hv 400, which is still lower than the hardness of the recast layer in this study.

3.4. Crystallographic data of the $(Fe,Mn)_3AlC_x$ carbide

The crystallographic data of $(Fe,Mn)_3AlC_x$ carbide measured by X-ray diffraction pattern is listed in Table III. The d-spacing and line intensity of the $(Fe,Mn)_3AlC_x$ carbide studied by Hale and Baker [23] are also listed in Table III. It reveals that the calculated lattice parameter increases slightly as the diffraction angle decreases. In fact, several systematic errors exist in the evaluation of lattice parameters, such as misalignment of the instrument, adsorption in the specimen and displacement of the specimen. The precise lattice parameters, a_o, of the $(Fe,Mn)_3AlC_x$ carbide are determined by extrapolating the calculated parameters against $\cos^2\theta/\sin\theta$ to reduce the systematic errors. The precise lattice parameter of the $(Fe,Mn)_3AlC_x$ phase evaluated by extrapolation is 0.3801 nm. According to Hale [23] and Sato [24], the lattice parameters of the $(Fe,Mn)_3AlC_x$ phase are 0.3797 nm and 0.372 to 0.378 nm, respectively. In this study, the values of lattice

TABLE II The average chemical compositions (wt%) of ferrite, austenite and recast layer in matrix, regions I and II of specimen H

Chemical composition	Cr	Mn	Al	C	Mo	Si	Cu	Fe
Ferrite in matrix	4.301	22.979	9.137	0.318	0.393	0.408	0.024	Bal.
Austenite in matrix	4.639	27.094	7.345	0.750	0.274	0.302	0.011	Bal.
Recast sublayers in region I	4.500	18.564	8.336	3.267	0.373	0.369	0.625	Bal.
γ recast zone in region I	4.194	23.203	8.773	2.341	0.301	0.374	0.071	Bal.
Austenite in region I	4.530	26.691	7.437	1.444	0.282	0.314	0.009	Bal.
Recast sublayers in region II	4.510	19.450	8.417	2.694	0.380	0.383	0.628	Bal.
γ recast zone in region II	4.268	23.371	8.277	1.874	0.353	0.348	0.091	Bal.
Ferrite in region II	3.995	21.917	9.227	0.717	0.372	0.392	0.021	Bal.
Austenite in region II	4.401	27.041	7.395	1.508	0.275	0.286	0.009	Bal.
Recast sublayers in average	4.505	19.007	8.377	2.981	0.377	0.376	0.627	Bal.
γ recast zone in average	4.231	23.287	8.525	2.108	0.327	0.361	0.081	Bal.

TABLE III Crystallographic data of the (Fe,Mn)$_3$AlC$_x$ phase

d-spacing (nm)	*hkl*	Lattice parameter (nm)	Observed intensity (%)	Normalized *d*-spacing (nm) by Hale[a]	Observed intensity by Hale[a]
0.3798	100	0.3798	9	0.3797	Weak
0.2680	110	0.3791	4	0.2685	Medium
0.2189	111	0.3792	80	0.2192	Strong
0.1901	200	0.3802	100	0.1898	Medium
0.1700	210	0.3800	5	–	–
0.1343	220	0.3798	20	0.1342	Medium
0.1146	311	0.3800	25	0.1145	Weak/medium
0.1098	222	0.3803	10	–	–

[a] See Ref. 23.

parameter of the (Fe,Mn)$_3$AlC$_x$ phase are 0.0004 nm to 0.0081 nm larger. The expansion of lattice parameter of (Fe,Mn)$_3$AlC$_x$ carbide structure is caused by the solid solution effect of Cr and minor amounts of Cu, Mo and Si in the carbide. It should be pointed out that the formation of a mass quantity (Fe,Mn)$_3$AlC$_x$ phase by electrical discharge machining of Fe-Mn-Al alloy system has never been reported before, although the formation of (Fe,Mn)$_3$AlC$_x$ phase in Fe-Mn-Al alloy has been investigated intensively in the literature [23–31]. In the early stage of developing Fe-Mn-Al austenitic alloys, James [25] and Kayak [26] first reported the isomorphous precipitation of (Fe,Mn)$_3$AlC$_x$ carbide with $\mathrm{L'1_2}$ crystal structure during age hardening at 723 to 923 K. According to Han and Choo [27–29], fine (Fe,Mn)$_3$AlC$_x$ carbides could be formed within the austenitic matrix of Fe-Mn-Al alloys during the rapid solidification (RS) process. In addition, the microstructures of as quenched Fe-Mn-Al-Si-C alloys were investigated by Chao [30] and Lee [31]. (Fe,Mn)$_3$AlC$_x$ carbides were found within the austenitic matrix during quenching by spinodal decomposition. However, the microstructure of the above-mentioned (Fe,Mn)$_3$AlC$_x$ carbides formed during the RS and quenching process are on the nanometer scale, which are quite different from the morphology observed in the present study. It is deduced that almost all of the workpiece material, melted due to high discharge energy during EDM will be resolidified rapidly on the machined surface. The extremely rapid solidification process, combined with high carbon from the cracking of the dielectric fluid, resulted in the novel coarse dendrite structure of (Fe,Mn)$_3$AlC$_x$ phase formed on the EDMed surface in this study.

4. Conclusions

1. Pulse duration (t_e) has greater influence than pulse current (I_e) on the thickness of the recast layer in EDMed dual phase Fe-24.0%Mn-8.3%Al-5.0%Cr-0.38%Si-0.34%Mo-0.45%C (wt%) alloy. When the pulse current is fixed, the average thickness of the recast layer increases with the pulse duration. However, the thickness of the recast layer remains constant as the pulse current increases from 8 to 12 A. The thickness of the recast layer is not influenced by discharge current for pulse durations in the range of 200 to 300 μs.

2. Several microcracks penetrate the recast layers and cleave deep into matrix in electical discharge machined Fe-Mn-Al alloy. Nevertheless, no microcracks are found in the matrix under the following electrical discharge machining conditions: $I_e = 10$–12 A and $t_e = 200$–300 μs.

3. Three novel solidification microstructures of the recast layer in EDMed Fe-Mn-Al alloy can be classified as (1) a dense and fine dendritic outermost sublayer, (2) a coarse dendritic intermediate sublayer and (3) an innermost γ recast zone. The chemical composition of the recast sublayers is Fe-19.007% Mn-8.377% Al-2.981% C-4.505% Cr-0.627% Cu-0.377% Mo-0.376% Si (wt%). The novel phase of the recast sublayers is identified as (Fe,Mn)$_3$AlC$_x$ carbide. The precise lattice parameter, a_o, of the (Fe,Mn)$_3$AlC$_x$ phase evaluated by extrapolation against $\cos^2\theta/\sin\theta$ is 0.3801 nm. A much higher microhardness of recast layer ranging from H_{mv} 548 to 574 is observed, which is attributed to the presence of (Fe,Mn)$_3$AlC$_x$ carbide.

Acknowledgements

The author would like to thank Mr. Kuen-Ling Wu for the EDM experiment. The financial support of NSC of Republic of China, Taiwan through contract No. NSC-89-2216-E-236-001 is also greatly appreciated.

References

1. L. C. LIM, L. C. LEE, Y. S. WONG and H. H. LU, *Mater. Sci. Technol* **3**(7) (1991) 239.
2. L. C. LEE, L. C. LIM, V. NARAYANAN and V. C. VENKATESH, *Int. J. Mach. Tool Manufact.* **28**(4) (1988) 359.
3. R. A. HADFIELD, US Patent 422403 (1887).
4. J. R. MITCHELL and M. E. POTTER, US Patent 3201230 (1965).
5. J. W. LEE, J. G. DUH and S. Y. TSAI, *Surf. Coat. Technol.* **153**(1) (2002) 59.
6. J. G. DUH, J. W. LEE and C. J. WANG, *J. Mater. Sci* **23** (1988) 2649.
7. J. G. DUH and J. W. LEE, *J. Electrochem. Soc.* **136**(3) (1989) 847.
8. B. K. ZUIDEMA, D. K. SUBRAMANYAM and W. C. LESLIE, *Metall. Trans.* A **18** (1987) 1629.
9. J. W. LEE, in Proceedings of 16th National Conference on Mechanical Engineering (The Chinese Society of Mechanical Engineering, Taiwan, Dec. 1999) Vol. 4, p.158.
10. C. H. KAHNG and K. P. RAJURKAR, *CIRP Ann.* **25**(1) (1977) 77.
11. A. G. MAMLIS, G. C. VOSNIAKOS, N. M. VAXEVANDIS and J. PROHSZKA, *J. Mech. Working Technol.* **15**(1) (1988) 335.

12. K. P. RAJURKAR and S. M. PANDIT, *J. Eng. Ind.* (Trans. ASME) **106**(2) (1984) 171.
13. L. MASSARELLI and M. MARCHIONNI, *Met. Technol.* **4**(2) (1977) 100.
14. J. S. SONI, *Wear* **177**(2) (1994) 71.
15. J. P. KRUTH, L. STEVENS, L. FROYEN and B. LAUWERS, *CIRP Ann.* **44**(1) (1995) 169.
16. C. P. TABRETT, *J. Mater. Sci. Let.* **15**(20) (1996) 1792.
17. H. K. LLOYD and R. H. WARREN, *J. Iron Steel Inst.* **203**(3) (1965) 238.
18. J. S. SONI and G. CHAKRAVERTI, *J. Mater. Proc. Technol.* **56**(1–4) (1996) 439.
19. Y. FUKUZAWA, YO KOJIMA, T. TANI, E. SEKIGUTI and N. MOHRI, *Mater. Manufact. Proc.* **10**(2) (1995) 195.
20. B. V. SHAROV and IZV. AKAD. NAUK, *SSSR Met. Topl.* **3** (1959) 148.
21. G. F. KOSOLAPOV and YU. D. TYAPKIN, *Metalloved. Term. Obrab. Met.* **41** (1955) 226.
22. M. A. E. R. MERDAN and R. D. ARNELL, *Surf. Eng.* **5**(2) (1989) 96.
23. C. E. HALE and A. J. BAKER, in “Alternate Alloying for Environmental Resistance,” edited by G. R. Smolik and Banerji (The Metallurgical Society of AIME, 1987) p. 67.
24. K. SATO, K. TAGAWA and Y. INOUE, *Metall. Trans.* A **21** (1990) 6.
25. P. J. JAMES, *J. Iron Steel Inst.* **207** (1969) 54.
26. G. L. KAYAK, *Met. Sci. Heat Treat.* **11**(2) (1969) 95.
27. K. H. HAN and W. K. CHOO, *Metall. Trans.* A **14** (1983) 973.
28. W. K. CHOO and K. H. HAN, *ibid.* **16** (1985) 5.
29. K. H. HAN and W. K. CHOO, *ibid.* **20** (1989) 205.
30. C. Y. CHAO, C. N. HWANG and T. F. LIU, *Scripta Metall.* **34**(1) (1996) 75.
31. J. W. LEE and T. F. LIU, *Mater. Chem. Phys.* **69** (2001) 192.

Received 24 June 2002
and accepted 8 January 2003